Ore Geology Reviews 101 (2018) 688–699

Contents lists available at ScienceDirect

Ore Geology Reviews

journal homepage: www.elsevier.com/locate/oregeorev

Geochronological, mineralogical and geochemical studies of sulfide mineralization in the Podong mafic-ultramafic intrusion in northern Xinjiang, western China

Shengchao Xue[a,b,*], Kezhang Qin[b], Chusi Li[c], Zhuosen Yao[b,d], Edward M. Ripley[c], Xinshui Wang[b]

[a] State Key Laboratory of Geological Processes and Mineral Resources, China University of Geosciences, Beijing 100083, China
[b] Key Laboratory of Mineral Resources, Institute of Geology and Geophysics, Chinese Academy of Sciences, Beijing 100029, China
[c] Department of Earth and Atmospheric Sciences, Indiana University, Bloomington, IN 47405, USA
[d] University of Chinese Academy of Sciences, Beijing 100049, China

ARTICLE INFO

Keywords:
Mafic-ultramafic rocks
Magmatic sulfide deposit
Zircon U-Pb dating
Sr-Nd-S isotopes
Central Asian Orogenic Belt

ABSTRACT

The Podong mafic-ultramafic intrusion is one of many Ni-Cu sulfide-mineralized intrusions in the Beishan-Tianshan Orogenic Belt in northern Xinjiang, western China. The temporal and lithological variations of the Ni-Cu mineralized intrusions in Beishan are much less constrained than those in Tianshan. This paper provides the first set of geochronological and geochemical data for the Podong magmatic sulfide deposit that is present in the Beishan region. The host intrusion is composed of lherzolite, troctolite, gabbronorite and gabbro. Ni-Cu mineralization occurs as disseminated sulfides in gabbronorite (± olivine). The zircon U-Pb age of gabbronorite is 270 ± 2.7 Ma, identical to the zircon U-Pb age of the nearby Poyi magmatic sulfide deposit that is hosted in troctolite and ultramafic rocks. These ages together define a new episode of Ni metallogeny in the Beishan region, which is ~10 Ma younger than that in the Tianshan region to the north. The Fo contents of olivine in the Podong mafic-ultramafic intrusion are from 76 to 87 mol%, lower than the values for the nearby Poyi mafic-ultramafic intrusion. The Podong mafic-ultramafic rocks are characterized by $\varepsilon_{Nd}(t)$ values from −0.61 to +1.92, low to elevated initial $^{87}Sr/^{86}Sr$ ratios (0.7055–0.7090), and pronounced negative Nb-Ta anomalies. The Sr-Nd isotope data indicate that the parental magma of the Podong intrusion experienced 0–13 wt% crustal contamination, which cannot fully account for the observed negative Nb-Ta anomalies in the rocks. Sulfur isotope compositions of the Podong deposit are similar to those of Pre-Permian sedimentary rocks in the area as well as typical mantle values. The results support the premise that fractional crystallization and assimilation of siliceous crustal materials may have played a key role in triggering sulfide saturation in the Podong magma, although the involvement of external sulfur cannot be completely ruled out. Like other Permian magmatic sulfide deposits in the Beishan-Tianshan Orogenic Belt, the PGE tenors of bulk sulfides in the Podong deposit are extremely low, indicating a severely PGE-depleted parental magma. The Cu/Pd ratios of the Podong magmatic sulfide deposit are significantly higher than the mantle values, consistent with previous sulfide segregation at depth. The results from the Podong magmatic sulfide deposit confirm that widespread Ni metallogeny in a convergent tectonic zone is very protracted and the mineralized lithologies are highly variable, which have significant implications for regional Ni-Cu exploration.

1. Introduction

Permian mafic-ultramafic intrusions are widespread in the Beishan-Tianshan Orogenic Belt in northern Xinjiang, western China. Some of these intrusions host important Ni-Cu ore deposits. In the Pobei area of the western Beishan region several small sulfide-mineralized mafic-ultramafic bodies, such as Poyi, Posan, Poshi and Podong, intruded a large gabbroic intrusion to form the Pobei mafic-ultramafic complex (Jiang et al., 2006; Su et al., 2013; Yang et al., 2014; Xue et al., 2016a; Ma et al., 2016). Recent zircon U-Pb age dating indicates that the Poyi magmatic sulfide deposit formed at ~270 Ma (Xue et al., 2016a), ~10 myr younger than those in the adjacent Tianshan region to the north (Han et al., 2004; Qin et al., 2011; Tang et al., 2011; Zhao et al., 2015). Such temporal variation, if verified, will improve our understanding of

* Corresponding author at: State Key Laboratory of Geological Processes and Mineral Resources, China University of Geosciences, Beijing 100083, China.
E-mail address: csuxsc@163.com (S. Xue).

https://doi.org/10.1016/j.oregeorev.2018.08.017
Received 6 February 2018; Received in revised form 2 August 2018; Accepted 14 August 2018
Available online 16 August 2018
0169-1368/ © 2018 Elsevier B.V. All rights reserved.

the relationship between tectonic evolution and Ni metallogeny in a convergent setting, which in turn may have significant implications for regional Ni exploration. Thus, we have carried out a geochronological study of the Podong magmatic sulfide deposit that has not been studied before. Another interesting question is the extent of lithological and compositional variations of this type of deposit in a small area, which is important for exploration targeting at a small scale. Previous studies show that sulfide mineralization in the nearby Poyi mafic-ultramafic intrusion is associated with wehrlites containing primitive olivine with Fo contents up to 89 mol%, and is severely depleted in PGEs, and has mantle-like S isotope compositions (Xue et al., 2016a). The similarity and difference between this deposit and the nearby Podong deposit should shed new light on the relationship between magma evolution and sulfide mineralization in the area. In this paper we report a new zircon U-Pb age for the Podong magmatic sulfide deposit, along with olivine chemistry, whole-rock chemical compositions, concentrations of trace elements and platinum-group elements (PGEs), whole-rock Sr-Nd isotopes, and sulfur isotopes of sulfide separates. We use these data to address the above-mentioned outstanding questions.

2. Geological background

The western part of the Beishan Orogenic Belt in northern Xinjiang is situated between the East Tianshan Orogenic Belt to the north and the Tarim Craton to the south (Fig. 1a, b). The Beishan region was an active continental margin in the Neoproterozoic and in the Early Paleozoic, as indicated by the distribution of ophiolites, and regional metamorphism and diverse magmatism during these periods in the region (Xiao et al., 2010; Guo et al., 2012). The Beishan Neoproterozoic-Paleozoic composite arc terrane is composed of Precambrian metamorphic complexes, Early Paleozoic marine sedimentary rocks, volcanic rocks and granitoids, and Late Paleozoic–Mesozoic terrestrial sedimentary rocks, plus Early Paleozoic ophiolites that mainly occur between Beishan and the East Tianshan accreted arc terrane to the north (Zuo et al., 1990; Zuo and Li, 1996; Yue et al., 2001; Xiao et al., 2010; Song et al., 2013). The Precambrian metamorphic complexes in the Beishan region are mainly comprised of marbles, crystalline limestones, slates, phyllites, metasandstones, leptynites, quartz schists and quartzites. The ages of the ophiolites vary from 536 to 320 Ma (Zhang and Guo, 2008; Wang, 2015, and reference therein). Based on these constraints, many researchers believe that subduction in the Beishan-Tianshan region finished by the end of the Carboniferous (e.g., Song et al., 2011; Zhang et al., 2011). However, a few researchers believe that subduction in the region lasted until Early Triassic (Ao et al., 2010; Xiao et al., 2010).

The Pobei mafic-ultramafic complex is situated at the westernmost end of the Beishan Orogenic Belt, spatially closely associated with the NE-trending regional Baidiwa fault (Figs. 1b, 2a). Country rocks to the complex are gneisses, marbles and schists (Fig. 2a). The Pobei intrusive complex consists of a large, older gabbroic intrusion with zircon U-Pb ages varying from 276 to 284 Ma (Qin et al., 2011; Ma et al., 2016; Xue et al., 2016a) and several small, younger mafic-ultramafic bodies. The Poyi mafic-ultramafic body is the only one that has been dated by zircon U-Pb method so far (~270 Ma: Xue et al., 2016a).

The Podong mafic-ultramafic intrusion is composed of lherzolite, troctolite, gabbronorite (olivine-bearing and olivine-free) and gabbro. Its surface exposure is ~1400 m in length, 80–400 m in width, with a downward extension > 600 m (Fig. 2b). Immediate country rocks are Late Paleozoic gabbros (Fig. 2b). To the south and east of the Podong intrusion, many dolerite dykes are present. One of these dykes has a zircon U-Pb age of ~281 Ma (Xue et al., 2016b). Several fragments of Proterozoic metamorphic rocks are present inside the intrusion. No chilled margins are present at the contacts between the intrusion and country rocks, including the fragments. The contacts between the gabbronorite and lherzolite within the intrusion are gradational (Fig. 2e). Two small gossan zones are present in the eastern part of the intrusion (Fig. 2b). Limited drilling indicates that Ni-Cu mineralization is present mainly as disseminated sulfides that are most closely associated with gabbronorite (Fig. 2c, d). Based on limited drilling to date it

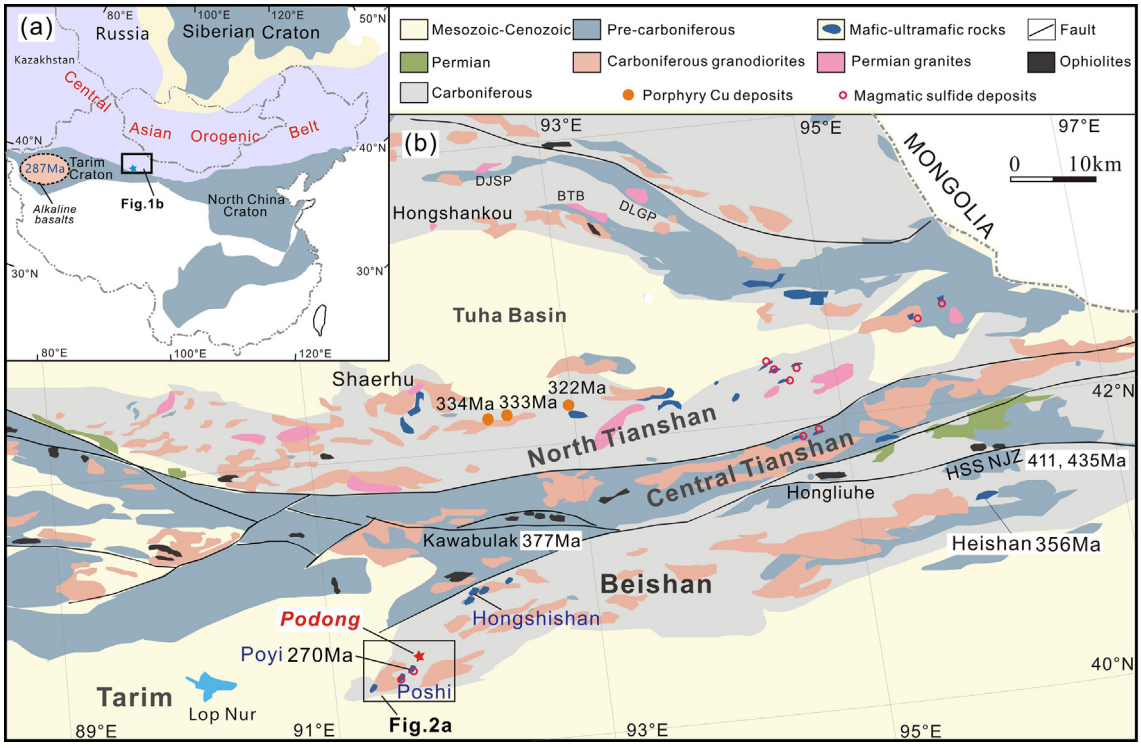

Fig. 1. (a) Simplified tectonic map of central Asia (after Jahn, 2004) and (b) distribution of Permian magmatic sulfide deposits in East Tianshan and Beishan. The geology of the Tianshan-Beishan region is after Xiao et al. (2004). Zircon U-Pb ages for mafic-ultramafic intrusions, ophiolites, granite plutons and porphyry Cu deposits are from a compilation by Mao et al. (2016).

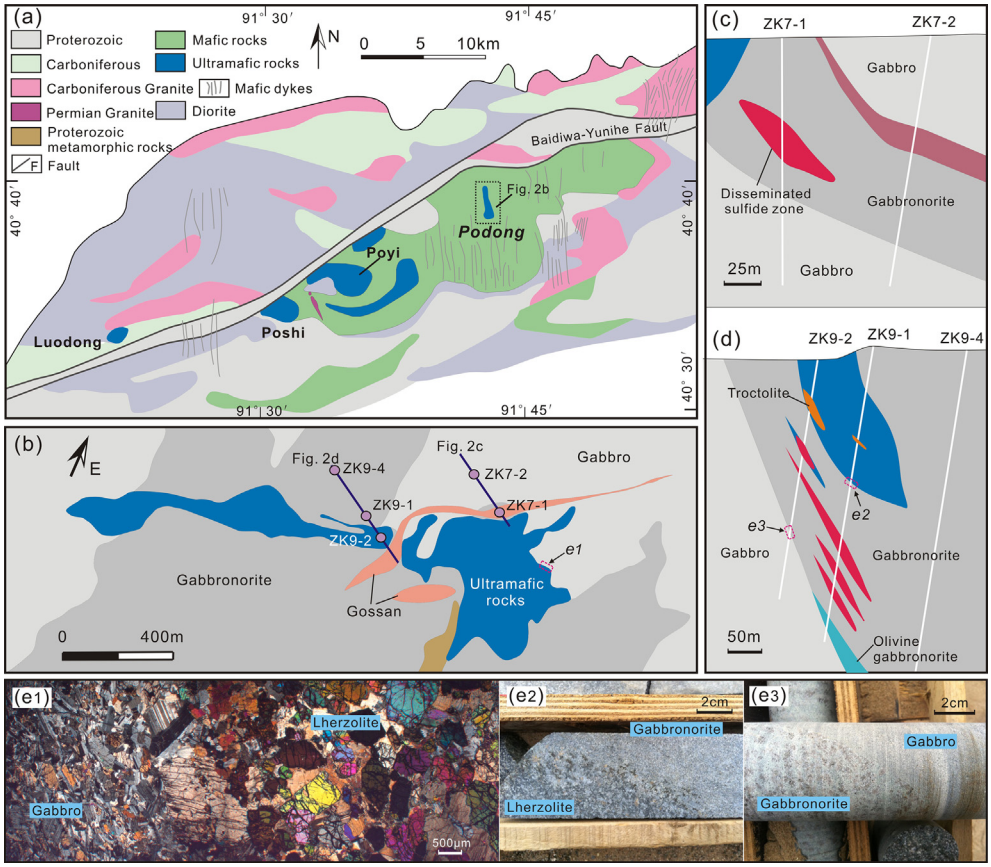

Fig. 2. Geological maps of the Pobei mafic-ultramafic complex (a) and the Podong sulfide-bearing mafic-ultramafic intrusion (b), and cross sections of the Podong intrusion (c, d), and the contacts between different rock types within the intrusion (e).

is suggested that the Podong magmatic sulfide deposit contains ~13.6 Mt of sulfide mineralization with 0.44 wt% Ni and 0.1 wt% Cu.

3. Sample descriptions

The samples used in this study were collected from two drill cores (ZK9-1 and ZK9-2) in the central part, and a drill core (ZK7-1) in the eastern part of the Podong mafic-ultramafic intrusion. Locations of the sampled drill cores and representative cross sections are shown in Fig. 2b-c-d. Our samples encompass all major rock types and the most important sulfide mineralization delineated by drilling to date.

Lherzolite is composed of 40–60 modal% olivine, 15–25 modal% clinopyroxene, and 10–20 modal% orthopyroxene, plus minor amounts of plagioclase (< 5 modal %), phlogopite, and Cr-spinel. Some small olivine grains are enclosed in anhedral clinopyroxene and to a lesser extent in orthopyroxene (Fig. 3a). Cr-spinel occurs as small inclusions within olivine and pyroxene crystals. Plagioclase and phlogopite occur in the interstitial spaces.

Troctolite contains 50–70 modal% olivine, 15–25 modal% plagioclase, 5–10 modal% clinopyroxene and orthopyroxene, and minor Cr-spinel. In this rock larger olivine crystals are surrounded by smaller plagioclase grains (Fig. 3b). Clinopyroxene and orthopyroxene occur as oikocrysts as well as in the interstitial spaces with plagioclase. Small and rounded sulfide inclusions enclosed in olivine crystals are present in troctolite as well as lherzolite (Fig. 3g, h).

Olivine gabbronorite contains 5–15 modal% olivine, 20–30 modal% clinopyroxene, 10–15 modal% orthopyroxene, 40–50 modal% plagioclase, and minor amounts of hornblende and biotite. This rock is fine-grained and has an equigranular texture (Fig. 3c). Olivine crystals commonly occur as anhedral grains with diameters varying from 0.5 to 2 mm. Clinopyroxene and plagioclase occur as intergrowths surrounding relatively large olivine crystals. Gabbronorite contains 20–35 modal% clinopyroxene, 10–30 modal% orthopyroxene, and 15–40 modal% plagioclase, plus < 5 modal% olivine and minor amounts of hornblende (Fig. 3d). Texturally this rock is similar to olivine gabbronorite, except for slightly larger grain sizes.

Gabbro is fine-grained and has an equigranular texture (Fig. 3e). It contains 20–30 modal% clinopyroxene, 55–75 modal% plagioclase, and < 5 modal% orthopyroxene, minor amounts of olivine and hornblende, plus variable amounts of Fe-Ti oxides (0–3 modal %) in places. Disseminated sulfide mineralization, which is predominately associated with gabbronorites, is composed of pyrrhotite, pentlandite, and chalcopyrite (Fig. 3f).

4. Sampling and analytical methods

4.1. Zircon U-Pb dating

Zircon grains were separated from ~6 kg of gabbronorite by conventional heavy liquid and magnetic separation techniques. The selected zircon grains were mounted in epoxy resin and polished. Cathodoluminescence (CL) images were obtained using a LEO1450VP scanning electron microscope with a MiniCL detector in the Institute of Geology and Geophysics, Chinese Academy of Sciences (IGGCAS), Beijing. The CL images were used to select pristine zircon grains free of visible inherited cores for U-Pb isotopic analysis. The isotopes of U and Pb in the selected zircon grains were determined using the CAMECA IMS 1280 ion microprobe in the IGGCAS. The analytical protocols and procedures are the same as those given in Li et al. (2009, 2010). The analytical errors are reported for one sigma uncertainty.

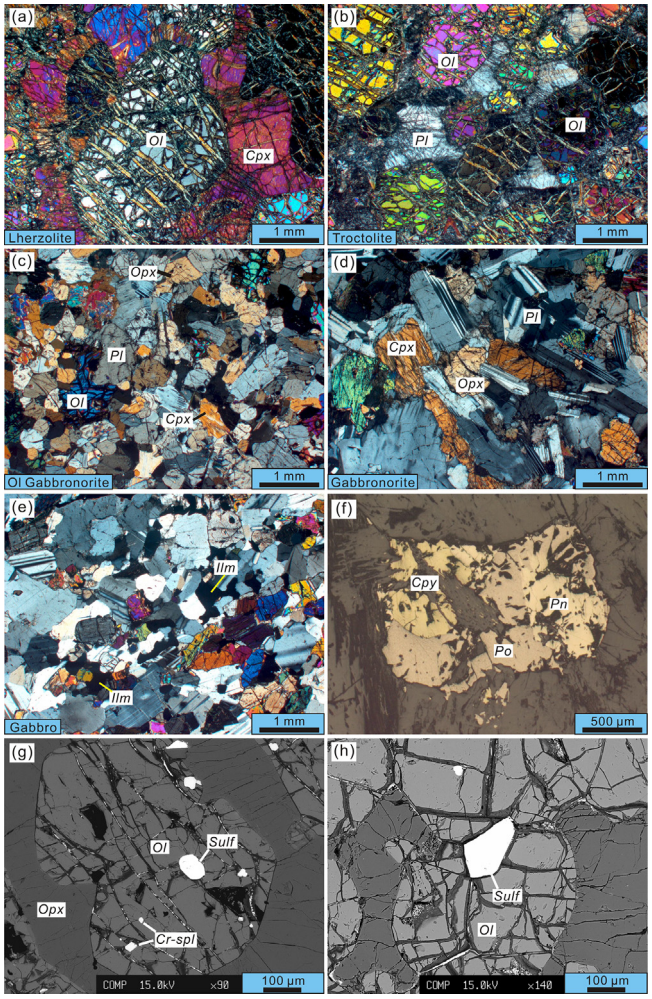

Fig. 3. Microphotographs of lherzolite (a), troctolite (b), olivine gabbronorite (c), gabbronorite (d), ilmenite-bearing gabbro (e), magmatic sulfide assemblage (f), and sulfide inclusion in olivine (g, h). *Ol*: olivine, *Cpx*: clinopyroxene, *Opx*: orthopyroxene, *Pl*: plagioclase, *Ilm*: Ilmenite, *Cr-Spl*: Cr spinel, *Cpy*: chalcopyrite, *Pn*: pentlandite, *Po*: pyrrhotite, *Sulf*: sulfide.

4.2. Mineral compositions

The compositions of major rock-forming minerals (olivine, clinopyroxene, orthopyroxene, plagioclase) and Cr-spinel were determined by wavelength dispersive X-ray analysis using a JEOL JXA8100 electron microprobe in the IGGCAS. The standards used in mineral analysis were albite for Na, diopside for Si, Ca, Mg, hematite for Fe, synthetic Cr_2O_3 for Cr, synthetic TiO_2 for Ti, orthoclase for K, synthetic Al_2O_3 for Al, synthetic MnO for Mn and synthetic NiO for Ni. The operating conditions were 15-kV accelerating voltage, 12-nA beam current, 5-μm beam diameter, and peak counting time of 30 s. Ni and Ca in olivine were analyzed by using a beam current of 20nA and a peak counting time of 100 s. The detection limit for Ni and Ca under these conditions was ~400 ppm and 200 ppm, respectively.

4.3. Whole-rock major and trace elements

An agate mortar was used to prepare the powder for all the bulk rock analyses in this study. The concentrations of major elements in whole rocks were measured using a Shimadzu XRF-1500 instrument in the IGGCAS. Loss-on-ignition (LOI) was determined by the weight loss of a powdered sample after one hour of heating at 1000 °C. The precision for the major elements is better than 2%. The accuracy and reproducibility were monitored using the Chinese national standard GSR3. The standard deviation of the standard was better than 1%.

Trace element concentrations in whole rocks were determined using ICP-MS methodology (Agilent 7500a with shielded torch) in the State Key Laboratory of Geological Processes and Mineral Resources, China University of Geosciences (Wuhan). The precision and accuracy are better than 5%, based on repeated analysis of the international rock standards (AGV-2, BHVO-1, BHVO-2, GSR-1, GSR-3, BCR-2). Sample digestion technique, the procedures of ICP-MS analysis, and the analytical precision and accuracy are the same as those given in Liu et al. (2008).

4.4. Whole-rock Sr-Nd isotopes

Whole-rock Sr-Nd isotopes were determined using a Finnigan Triton thermo-ion mass spectrometer in the Wuhan Sample Solution Analytical Technology Co., Ltd. The analytical procedures are the same as those given in Rudnick et al. (2004). The measured $^{87}Sr/^{86}Sr$ and $^{143}Nd/^{144}Nd$ ratios are normalized to $^{86}Sr/^{88}Sr = 0.11940$ and $^{146}Nd/^{144}Nd = 0.721900$, respectively. Total analytical blanks were 5×10^{-11} g for Sm and Nd and $(2–5) \times 10^{-10}$ g for Rb and Sr. The average NBS-987 standard gave $^{87}Sr/^{86}Sr = 0.710241 \pm 0.000012$ (2σ), and the $^{143}Nd/^{144}Nd$ ratio of the JNdi-1 standard measured during the sample runs was 0.512115 ± 0.000007.

4.5. Chalcophile elements (Ni, Cu, S and PGE)

The concentrations of S, and Ni and Cu in sulfide-bearing rocks were analyzed using a LECO C-S Analyzer and by an ICP-AES instrument in the ALS Chemex Laboratory, Guangzhou, respectively. The concentrations of PGE were determined by isotope-dilution ICP-MS technique in the State Key Laboratory of Ore Deposit Geochemistry, Institute of Geochemistry, Chinese Academy of Sciences, Guiyang, following the procedures given in Qi et al. (2007, 2011). The total procedural blanks were 0.009 ng for Ir (lowest among all PGE) and 0.033 ng for Pd (highest among all PGE). The detection limits were 0.004 ppb for Ir (lowest among all PGE) and 0.012 ppb for Pd (highest among all PGE). The precision and accuracy of the measurements for the concentrations > 0.2 ppb are better than 10%.

4.6. Sulfur isotopes

Sulfur isotope analysis of sulfide separates was carried out at Indiana University-Bloomington, USA, following the procedures described in Studley et al. (2002). Sulfide minerals (pentlandite, chalcopyrite and pyrrhotite) were drilled from polished sections using a 0.75-mm carbide bit. Sample powders of 0.1–0.2 mg were then placed in tin cups with 1–1.5 mg of vanadium pentoxide (V_2O_5) and combusted at 1800 °C, with a reactor column temperature of 1010 °C. Measurements of produced SO_2 were made using a Finnigan Delta V stable isotope ratio mass spectrometer, with results reported in delta notation (with multiplication by 1000 for conversion to per mil values) relative to Vienna-Canyon Diablo Troilite. Analytical uncertainty was less than ± 0.05%, and sample reproducibility was within ± 0.2%. Sulfide standards utilized included IAEA-S1 (with a defined value of −0.3% V-CDT), and IAEA-S2 and IAEA-S3 with values of 21.7% and −31.3%, both on the SO_2 scale.

5. Analytical results

5.1. Zircon U-Pb age

Zircon U-Pb isotope data for the Podong gabbronorite are listed in Supplementary Table 1 (Table S1). The selected zircon grains are euhedral and prismatic with variable lengths from 60 to 150 μm and aspect ratios from 1:1 to 4:1. Some have oscillatory zoning and others are dark and homogeneous in CL images (Fig. 4). The contents of U and Th

Table 1
Sr-Nd isotopes of the Podong mafic-ultramafic intrusion.

Sample no.	Rock type	Rb (ppm)	Sr (ppm)	$^{87}Rb/^{86}Sr$	$^{87}Sr/^{86}Sr$	± 2σ	$(^{87}Sr/^{86}Sr)_i$	Sm (ppm)	Nd (ppm)	$^{147}Sm/^{144}Nd$	$^{143}Nd/^{144}Nd$	± 2σ	$\varepsilon_{Nd}(t)$
9-1-538	Gabbronorite	2.22	344	0.018664	0.707579	0.000009	0.707507	0.51	1.54	0.197676	0.512649	0.000046	0.17
9-2-185.5	Ol Gabbronorite	0.71	286	0.007183	0.707994	0.00001	0.707966	0.48	1.4	0.209095	0.512629	0.000031	-0.61
9-1-140	Troctolite	3.02	59.5	0.146708	0.70606	0.000013	0.705496	0.89	3.09	0.173988	0.512602	0.000036	0.09
9-2-130	Troctolite	2.02	115	0.050843	0.706015	0.000007	0.705820	0.49	1.48	0.202663	0.512746	0.000043	1.91
9-1-223	Pl lherzolite	1.09	85.2	0.037147	0.706022	0.000008	0.705879	0.46	1.57	0.177179	0.512702	0.000037	1.92

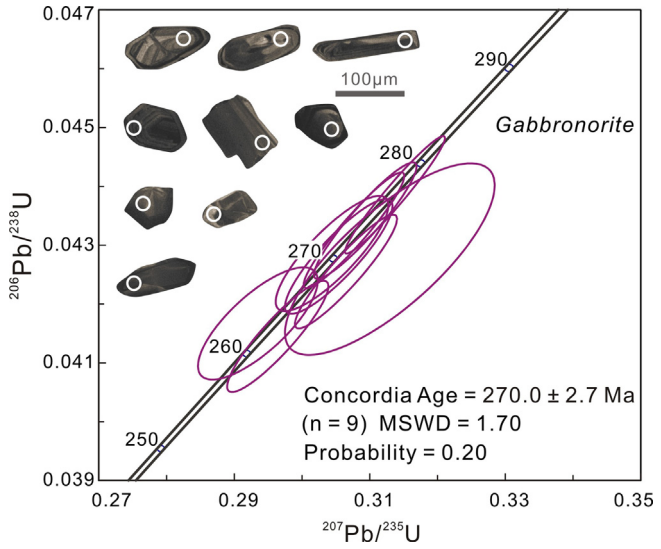

Fig. 4. CL images of selected zircon grains and Concordia diagrams of zircon U-Pb isotopes for the Podong gabbronorite.

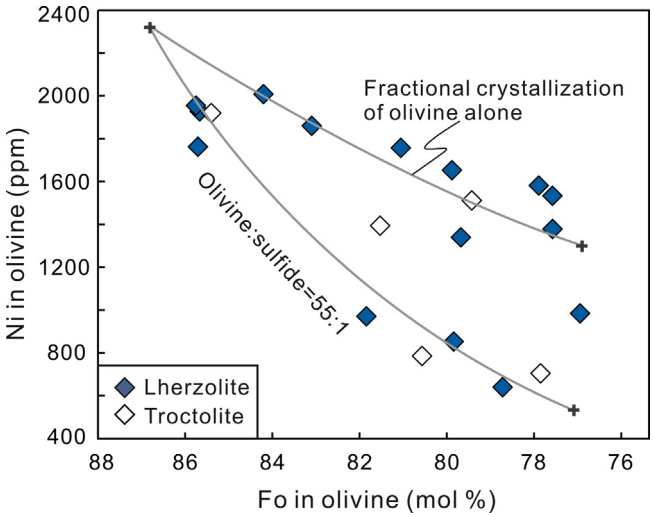

Fig. 5. Compositional variations of olivine crystals from the Podong intrusion. See the text for detailed modeling.

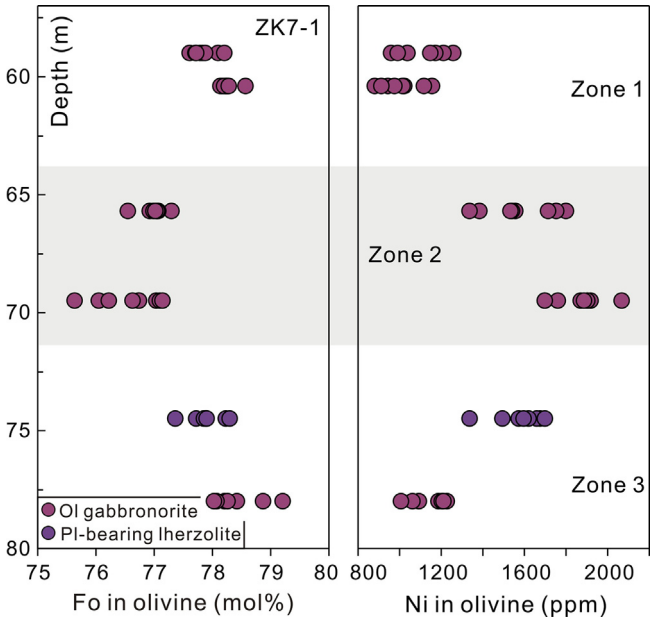

Fig. 6. Olivine stratigraphic compositional variations in drill core ZK7-1.

for nine grains vary from 676 to 2247 ppm and from 135 to 1026 ppm, respectively, with Th/U ratios from 0.20 to 0.49. Data reduction using the Isoplot 3.75 program of Ludwig (2012) yields a concordant U-Pb age of 270.0 ± 2.7 Ma (MSWD = 1.70, probability = 0.20) (Fig. 4), identical to the age of the nearby Poyi magmatic Ni-Cu sulfide deposit (Xue et al., 2016a).

5.2. Mineral compositions

The compositions of important rock-forming minerals such as olivine, orthopyroxene, clinopyroxene, plagioclase, and Cr-spinel in the Podong intrusion are given in Table S2. The variations of Fo and Ni contents in olivine in sulfide-barren samples from the Podong intrusion are illustrated in Fig. 5, showing a weak positive Fo-Ni correlation that is generally consistent with fractional crystallization plus "trapped liquid" shift (Li et al., 2007). Olivine crystals in lherzolite and troctolite contain forsterite (Fo) from 76.9 to 86.5 mol%. Olivine crystals in olivine gabbronorite have Fo contents ranging from 75.6 to 79.2 mol%.

The stratigraphic variations of olivine compositions in drill core ZK7-1 that is significantly sulfide mineralized (Fig. 2b, c) are illustrated in Fig. 6. This drill core can be further divided into three zones, with each zone showing a clear negative Ni-Fo correlation that is generally consistent with Fe-Ni exchange reactions between olivine and sulfide liquid. The middle zone is characterized by the highest Ni contents coupled with the lowest Fo contents.

The En contents [100 × Mg/(Mg + Fe^{2+} + Ca), molar] of clinopyroxene in lherzolite and troctolite in the Podong intrusion are between 46 and 54. Clinopyroxene in coexisting olivine gabbronorite and gabbronorite has slightly lower En contents, varying from 43 to 51. The En contents of orthopyroxene in lherzolite and troctolite are from 77 to 86. Orthopyroxene in gabbronorite has En contents varying from 70 to 79. The An contents of plagioclase in the Podong intrusion vary from 59 to 79 mol%.

Cr-spinel inclusions enclosed in olivine, clinopyroxene and orthopyroxene in the Podong intrusion contain 16.1–29.4 wt% Al_2O_3, 31.2–46.7 wt% Cr_2O_3 and 3.4–9.5 wt% MgO, with Cr# [100 × Cr/(Cr + Al), molar] varying between 42 and 66. A regional and global comparison is illustrated in Fig. 7. The compositions of Cr-spinel from the Podong intrusion are similar to those from other Permian sulfide-mineralized mafic-ultramafic intrusions in the Beishan-Tianshan region, such as Huangshandong (Mao et al., 2015) and Poyi (Xue et al., 2016a). Cr-spinel crystals from all these intrusions mostly plot in the

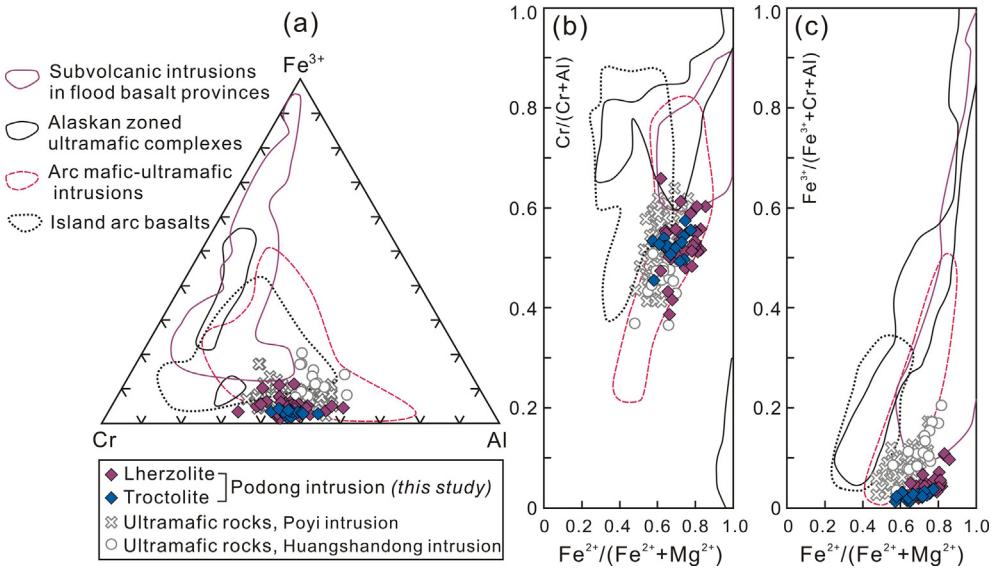

Fig. 7. Fe^{3+}-Cr-Al ternary plot (a), and Cr/(Cr + Al) and $Fe^{3+}/(Fe^{3+} + Cr + Al)$ versus $Fe^{2+}/(Fe^{2+} + Mg^{2+})$ plots (b, c) for Cr-spinel from the Podong intrusion. Sources of data for comparison: the ~270 Ma Poyi mafic-ultramafic intrusion in Beishan (Xue et al., 2016a), the ~274 Ma Huangshandong mafic-ultramafic intrusion (Mao et al., 2015), arc mafic-ultramafic intrusions (Thakurta et al., 2008; Li et al., 2013, 2015), and subvolcanic intrusions in flood basalt provinces, Alaskan-zoned ultramafic complexes and island arc basalts (Barnes and Roeder, 2001; Kamenetsky et al., 2001).

field for those from arc mafic-ultramafic intrusions in the world (Fig. 7) (Barnes and Roeder, 2001).

5.3. Whole-rock major and trace elements

The abundances of major and trace elements in sulfide-barren samples from the Podong mafic-ultramafic intrusion are listed in Table S3. The LOI-free (LOI, loss on ignition) compositions are compared to the compositions of major rock-forming minerals in Fig. 8. The comparison reveals that the compositions of lherzolite, troctolite and gabbronorite are mainly controlled by the abundances of olivine-pyroxenes, olivine-plagioclase and pyroxenes-plagioclase, respectively, consistent with petrographic analyses.

The mantle-normalized trace element patterns for the Podong mafic-ultramafic rocks are illustrated in Fig. 9. The abundances of the incompatible trace elements in the Podong mafic-ultramafic rocks are significantly lower than the values in the associated mafic dykes. However, they are all characterized by pronounced negative Nb-Ta anomalies with the exception of Fe-Ti oxide gabbros (Fig. 9a). The Fe-Ti oxide gabbros show positive Nb-Ta anomalies instead because these

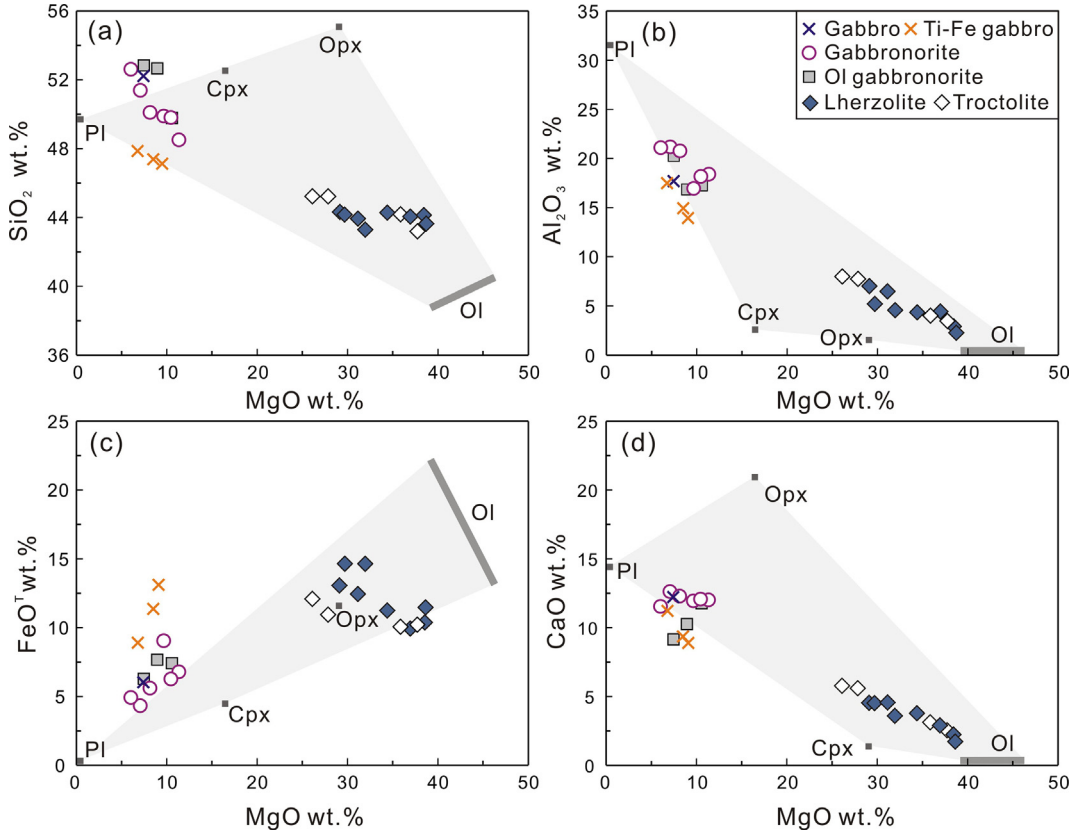

Fig. 8. Compositional comparison of whole rocks with major rock-forming minerals in the Podong mafic-ultramafic intrusion. The mineral abbreviations are same as in Fig. 3.

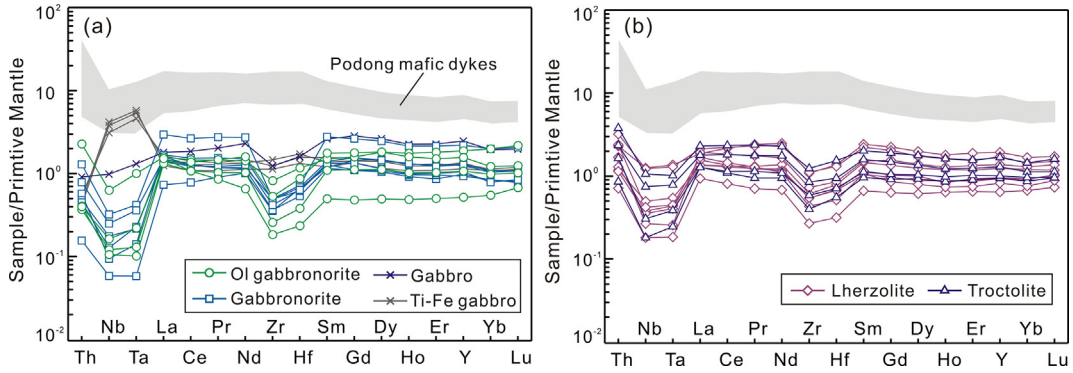

Fig. 9. Mantle normalized incompatible element patterns for gabbro, Ti-Fe gabbro, gabbronorite and olivine gabbronorite (a), and for lherzolite and troctolite (b) in the Podong intrusion. The fields of the Podong mafic dykes are from Xue et al. (2016b). The normalization values are from Palme and O'Neill (2014).

elements are compatible in Fe-Ti oxides, as indicated by experimental results (e.g., Nielsen and Beard, 2000).

5.4. Sr-Nd isotopes

Sr-Nd isotopes of the Podong mafic-ultramafic rocks are listed in Table 1. The calculated initial $(^{87}Sr/^{86}Sr)_i$ ratios and $\varepsilon_{Nd}(t)$ based on a formation age of 270 Ma from zircon U-Pb isotopes are from 0.7055 to 0.7090 and from −0.61 to +1.92, respectively. These values plot below the ranges for the coeval Poyi mafic-ultramafic intrusion and the associated Podong mafic dykes (Fig. 10a).

5.5. Chalcophile elements

The concentrations of Cu, Ni and PGE in sulfide-bearing (> 0.4 wt% S) and sulfide-barren (< 0.4 wt% S) rocks from the Podong mafic-ultramafic intrusion are listed in Table 2. The Ni/Cu ratios for sulfide-bearing samples vary from 1.8 to 3.1, within the range for the Permian magmatic Ni-Cu sulfide deposits in East Tianshan (see summary in Qin et al., 2011). The correlations between chalcophile element and S contents in whole rock samples from the Podong intrusion are illustrated in Fig. 11. The abundances of all chalcophile elements show a good positive correlation with S contents. We have calculated the metal tenors, or the concentrations of metals in the bulk sulfides (recalculated to 100% sulfides) of these samples using the equation of Barnes and Lightfoot (2005). The mantle-normalized patterns of these samples are illustrated in Fig. 12, which reveal that the bulk sulfide compositions of the Podong deposit are characterized by fractionated PGE patterns plus depletions of PGE relative to Ni and Cu.

5.6. Sulfur isotopes

Sulfur isotope compositions of the Podong magmatic sulfide deposit are listed in Table 3. Ten samples are from the gabbronorite zone and the rest are from the lherzolite and troctolite zones. The $\delta^{34}S$ values vary from 0.82 to 2.02%, overlapping the range for other Permian magmatic sulfide deposits in the Pobei area ($\delta^{34}S$ = −2.0 to +1.2%: Su et al., 2013; Xia et al., 2013). The whole range is similar to that of typical mantle values (0 ± 2%: see summary in Ripley and Li, 2013).

6. Discussion

6.1. Onset of sulfide saturation during magma evolution

To determine the temporal relationship between magma evolution and sulfide saturation we need to know the composition of the parental magma for the most primitive rocks in the intrusion. Given the similar age between the Podong and Poyi intrusions, plus their spatial proximality, the estimated parental magma for the Poyi intrusion (Xue et al., 2016a) may be used for the Podong intrusion. However, the complete lithologies of these two intrusions are different. The Podong intrusion mainly contains lherzolite and olivine gabbronorite, with minor troctolite, websterite, norite and Fe-Ti gabbro, whereas the Poyi intrusion is

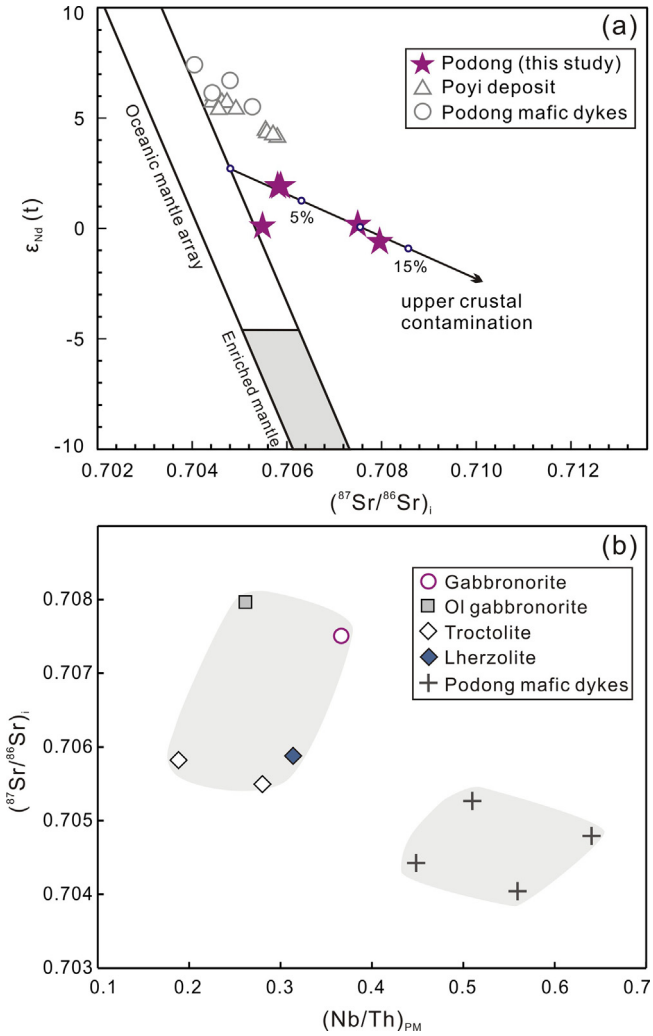

Fig. 10. $(^{87}Sr/^{86}Sr)_i$ vs. $\varepsilon_{Nd}(t)$ (a) and mantle-normalized Nb/Th (b). The data for the Poyi deposit and the Podong mafic dykes are from Xue et al. (2016a, b). End-member compositions for modelling: upper crust, 27 ppm Nd, 320 ppm Sr, $\varepsilon_{Nd}(t)$ = −8, $(^{87}Sr/^{86}Sr)_i$ = 0.715; mantle-derived magma, 9.8 ppm Nd, 97 ppm Sr, $\varepsilon_{Nd}(t)$ = 2.8, $(^{87}Sr/^{86}Sr)_i$ = 0.7048. The oceanic mantle array is from Zindler and Hart (1986). The normalization values are from Palme and O'Neill (2014).

Table 2
Concentrations of S, Ni, and Cu (wt%) and PGE (ppb) in the Podong intrusion.

Sample no.	Rock type	S	Ni	Cu	Co	Ir	Ru	Rh	Pt	Pd
Disseminated										
9-2-162	Lherzolite	0.40	0.15	0.05	0.02	0.07	0.07	0.06	0.96	1.31
9-2-163.4	Lherzolite	1.84	0.46	0.15	0.01	0.43	0.57	0.60	2.66	4.15
9-2-164.3	Troctolite	1.84	0.47	0.17	0.03	0.5	0.65	0.39	0.79	3.42
7-1-60.4	Ol gabbronorite	0.59	0.10	0.04	0.00	0.12	0.10	0.16	2.63	3.11
7-1-62.7	Ol gabbronorite	2.42	0.38	0.15	0.01	0.65	0.49	0.44	1.82	8.55
7-1-65.7	Ol gabbronorite	0.65	0.14	0.05	0.03	0.17	0.22	0.23	1.12	2.00
7-1-69.5	Ol gabbronorite	1.36	0.27	0.09	0.01	0.45	0.51	0.33	4.44	6.23
7-1-78	Ol gabbronorite	3.84	0.64	0.23	0.01	1.01	0.76	1.38	20.2	34.7
9-2-160.4	Gabbronorite	1.04	0.11	0.06	0.02	0.15	0.20	0.23	0.63	1.47
7-1-56.2	Gabbronorite	1.94	0.34	0.11	0.03	0.61	0.75	0.65	4.34	6.61
7-1-57	Gabbronorite	3.65	0.59	0.21	0.03	1.04	1.16	1.23	19.3	11.5
7-1-57.8	Gabbronorite	2.71	0.48	0.17	0.02	0.97	0.91	0.72	10.6	10.5
7-1-59	Gabbronorite	1.90	0.32	0.11	0.02	0.54	0.32	0.62	6.36	8.26
7-1-86.4	Gabbronorite	1.54	0.27	0.09	0.05	0.88	0.61	1.38	18.5	18.8
Sulfide-barren										
9-2-151.5	Ol gabbronorite	0.26	0.05	0.02	0.01	0.04	0.07	0.07	0.28	0.71
7-1-74.5	Lherzolite	0.14	0.12	0.01	0.00	0.11	0.17	0.07	0.39	0.48

composed of dunite and wehrlite, with minor troctolite, olivine clinopyroxenite and olivine gabbro. Sulfide mineralization dominantly occurs in olivine gabbronorite and lherzolite in the Podong intrusion whereas it occurs in wehrlite within the Poyi intrusion. Although the crystallization sequence inferred from the major rock types in both intrusions are similar, the Sr-Nd isotope compositions are significantly different between these two coeval intrusions, indicating that they do not share the same mantle source (Fig. 10a). Therefore, it is better to estimate the parental magma for the Podong intrusion using the data from this intrusion and use the result for petrological modeling such as olivine fractional crystallization and sulfide segregation that took place in the Podong magmatic system.

Li and Ripley (2011) introduced a method to estimate the liquid composition for olivine cumulates. This method is applicable to some lherzolite samples from the Podong intrusion, such as those containing the most primitive olivine, high Zr, and low CaO and Al_2O_3 abundances. We have selected a sulfide-barren lherzolite sample for modelling. In our calculations we adapted the experimental olivine-liquid Fe-Mg exchange coefficient [K_D, $(FeO/MgO)_{olivine}/(FeO/MgO)_{liquid}$] of 0.34 from Matzen et al. (2011) for tholeiites. The presence of cumulus plagioclase in places in the Podong intrusion and the nearly flat REE mantle-normalized patterns are consistent with a tholeiitic parental magma for this intrusion. The estimated oxide contents in parental magma for the Podong lherzolite are included in Table S3. We have used the MELTS program of Ghiorso and Sack (1995) to simulate the fractional crystallization of such magma at 1 kb (or at depth of ~3 km) and an oxidation state of QFM +0.5 (one half logarithm unit above the fayalite-magnetite-quartz buffer). The oxidation state for the Podong magmatic system was estimated using the equation of Barnes et al. (2013) that is based on the empirical relationship between the oxidation state and Fe-Ni exchange coefficient (K_D) between olivine and sulfide liquid. The common occurrence of hornblende and phlogopite in the intrusion indicates that the parental magma contained water, although the exact amount cannot be determined. Thus, we have added 1 wt% H_2O to the magma in our simulation. Under these conditions, olivine containing ~87 mol% Fo starts to crystallize from the magma at 1241 °C. Clinopyroxene appears on the liquidus with olivine at 1163 °C. The results from the MELTS simulation include the relationship between olivine Fo contents and the degrees of fractional crystallization. The relationship between olivine Ni and Fo contents can be determined using the Rayleigh fractionation equation and the partition coefficient of Ni between olivine and magma estimated using the equation of Li and Ripley (2010). The modeling results are compared with actual observation in Fig. 5, which shows that the variations of olivine Fo-Ni contents in the Podong sulfide-barren rocks cannot be explained by olivine fractional crystallization alone. Cotectic sulfide segregation during olivine crystallization is required to explain the whole range of olivine compositional variation in these rocks, consistent with the occurrence of rounded sulfide inclusions in olivine crystals in the Podong olivine cumulates (Fig. 3g, h). Using a widely accepted partition coefficient of 500 for Ni between sulfide liquid and magma (see summary in Naldrett, 2011), our calculation shows that a mass olivine/sulfide ratio of ~55 can well explain olivine with lower Ni contents in the intrusion (Fig. 5). The textures and modeling results indicate that sulfide saturation in the Podong magmatic system occurred no later than the crystallization of the most primitive olivine in the intrusion.

6.2. Crustal contamination and source characteristics

We have used whole-rock Sr-Nd isotopes to constrain crustal contamination. Mixing calculations indicate that the Podong magma experienced 0 to13 wt.% assimilation of the upper crust (Fig. 10a). It is well known that the bulk crust is highly enriched in light REE and Th but severely depleted in Nb as compared to the primitive mantle. This raises the possibility that the observed negative Nb anomaly in the Podong mafic-ultramafic rocks may have solely resulted from crustal contamination. If this is true, a negative correlation between the mantle-normalized Nb/Th and $(^{87}Sr/^{86}Sr)_i$ should be expected. As shown in Fig. 10b, no such correlation is present in the Podong mafic-ultramafic rocks, indicating that crustal contamination is not the only reason for the observed negative Nb anomaly in these rocks. Similarly, the associated mafic dykes, which show variable and minor degrees of crustal contamination based on Sr-Nd isotopes (Fig. 10a), also do not show any correlation between the mantle-normalized Nb/Th and $(^{87}Sr/^{86}Sr)_i$ (Fig. 10b). Therefore, we conclude that part of the observed negative Nb anomaly in the Permian mafic-ultramafic rocks is a primary signature of the magma. Subduction-related magma is commonly characterized by pronounced negative Nb-Ta anomalies (e.g., Class and Le Roex, 2008). It is widely accepted that the Permian mafic-ultramafic intrusions in the Beishan-Tianshan Orogenic Belt formed ~30 Ma after the end of subduction (Mao et al., 2014, 2016). In this context, it is inferred that the mantle source of these intrusions was metasomatized by slab-derived fluids and/or subducted sediment-derived melt during the previous subduction processes.

6.3. Cause of sulfide saturation

Addition of external sulfur and assimilation of siliceous crustal materials are important for the formation of many magmatic sulfide deposits worldwide (e.g., Naldrett, 2011; Ripley and Li, 2013). Sulfur

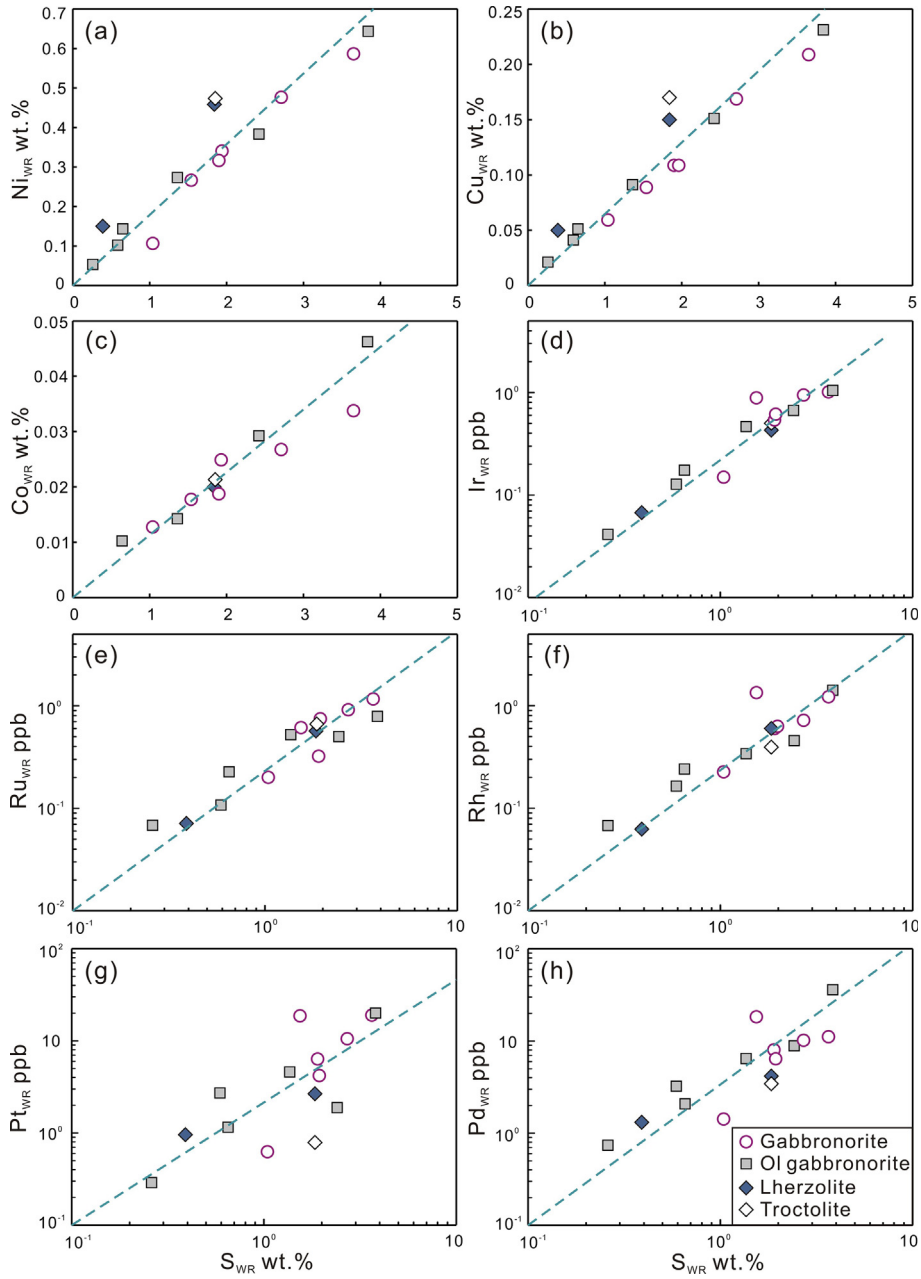

Fig. 11. Plots of chalcophile element concentrations versus sulfur contents in whole rocks in the Podong sulfide-bearing mafic-ultramafic intrusion.

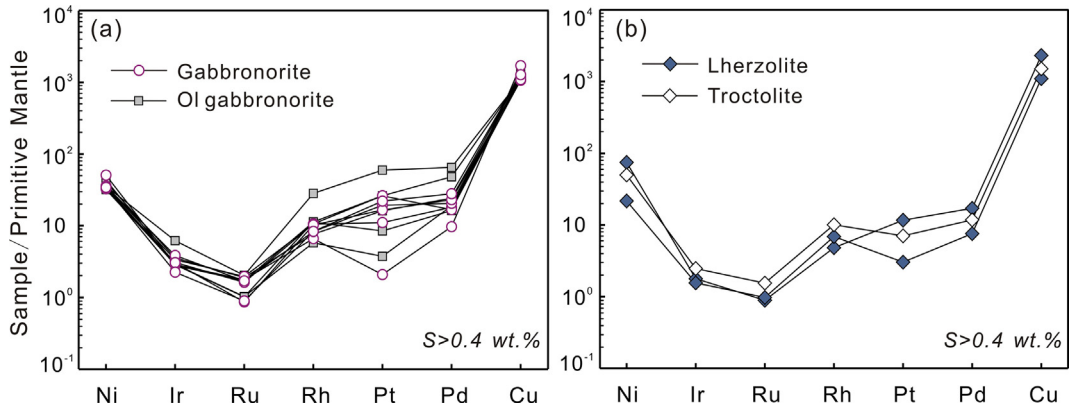

Fig. 12. Primitive-normalized patterns of metal tenors in the Podong magmatic sulfide deposit. The primitive mantle values are from Palme and O'Neill (2014).

Table 3
Sulfur isotopes of the Podong sulfide-bearing intrusion.

Sample no.	Rock type	Mineralization	$\delta^{34}S$ (%)
7-1-74.5	Lherzolite	Disseminated sulfides	0.99
9-2-162	Lherzolite	Disseminated sulfides	1.25
9-2-163.4	Lherzolite	Disseminated sulfides	0.98
9-2-164.3	Troctolite	Disseminated sulfides	0.82
7-1-60.4	Ol Gabbronorite	Disseminated sulfides	1.9
7-1-62.7	Ol Gabbronorite	Disseminated sulfides	1.63
7-1-65.7	Ol Gabbronorite	Disseminated sulfides	1.11
7-1-69.5	Ol Gabbronorite	Disseminated sulfides	1.29
7-1-78.0	Ol Gabbronorite	Disseminated sulfides	1.62
7-1-56.2	Gabbronorite	Disseminated sulfides	2.02
7-1-57.8	Gabbronorite	Disseminated sulfides	1.8
7-1-59.0	Gabbronorite	Disseminated sulfides	2.01
7-1-86.4	Gabbronorite	Disseminated sulfides	1.42
9-2-160.4	Gabbronorite	Disseminated sulfides	1.49

isotopes of the Podong magmatic sulfide deposit ($\delta^{34}S$, +0.82 to +2.02%) are not significantly different from typical mantle values (0 ± 2%: see summary in Ripley and Li, 2013) or the values for the country rocks of Permian mafic-ultramafic intrusions in the area ($\delta^{34}S$, −0.78 to 0.05%, Su et al., 2013). Thus, it is difficult to determine whether external sulfur was involved in the genesis of sulfide mineralization in the Podong mafic-ultramafic intrusion. On the other hand, $(^{87}Sr/^{86}Sr)_i$ ratios (0.7055–0.7090) and $\varepsilon_{Nd}(t)$ values (−0.61 to +1.92) provide clear evidence for assimilation of siliceous crustal materials by the parental magma of the Podong mafic-ultramafic intrusion (Fig. 10a). As shown in the figure, mixing calculations indicate that the parental magma of the Podong mafic-ultramafic intrusion experienced from 0 to 13 wt% assimilation of siliceous continental crustal rocks; the addition of siliceous crustal material is also consistent with the presence of orthopyroxene in the rocks. The assimilation of siliceous crust appears to have played a role in the genesis of the Podong magmatic sulfide deposit, but we cannot rule out the involvement of external sulfur due to inconclusive sulfur isotope data.

6.4. Controls on PGE variations

Positive correlation between chalcophile elements (Ni, Cu, Co and PGE) and S in whole rock samples from the Podong deposit (Fig. 11) indicates that the distribution of these elements in the intrusion is mainly controlled by magmatic sulfide mineralization. IPGE (Ir, Ru, Rh) and PPGE (Pt, Pd) behave similarly during sulfide liquid segregation from magma (e.g., Naldrett, 2011; Mungall and Brenan, 2014) but differently during fractional crystallization of monosulfide solid solution (MSS) from sulfide liquid on cooling (e.g., Li et al., 1996). Good positive correlations between Ir and Pt or Pd tenors in the Podong deposit (Fig. 13) indicate that these samples did not experience significant MSS fractional crystallization. Poorer correlation between Pt and Ir than between Pd and Ir is a manifestation of Pt anomalies in some of the samples (Fig. 12). Such anomalies are commonly due to crystallization of Pt minerals from magmatic sulfide liquid on cooling (Prichard et al., 2013) or Pt redistribution during post-magmatic hydrothermal alteration (Tang et al., 2011), or both. Due to this uncertainty, Pd is preferred for modeling of the sulfide-liquid segregation process using the R-equation (R, sulfide liquid/silicate liquid mass ratio) of Campbell and Naldrett (1979). In this equation the initial concentration of a metal in magma, its partition coefficient (D value) between sulfide liquid and silicate magma, and the R-factor are independent variables. Due to extremely high D values for PGE (e.g., Mungall and Brenan, 2014), the concentrations of these metals in a sulfide liquid depend on both R factors and their initial contents in magma. Hence, it is important to set a minimum R-factor using other chalcophile elements with lower D values such as Ni or Cu. Due to the effects of olivine fractional crystallization and subsolid Fe-Ni exchange between olivine and sulfide

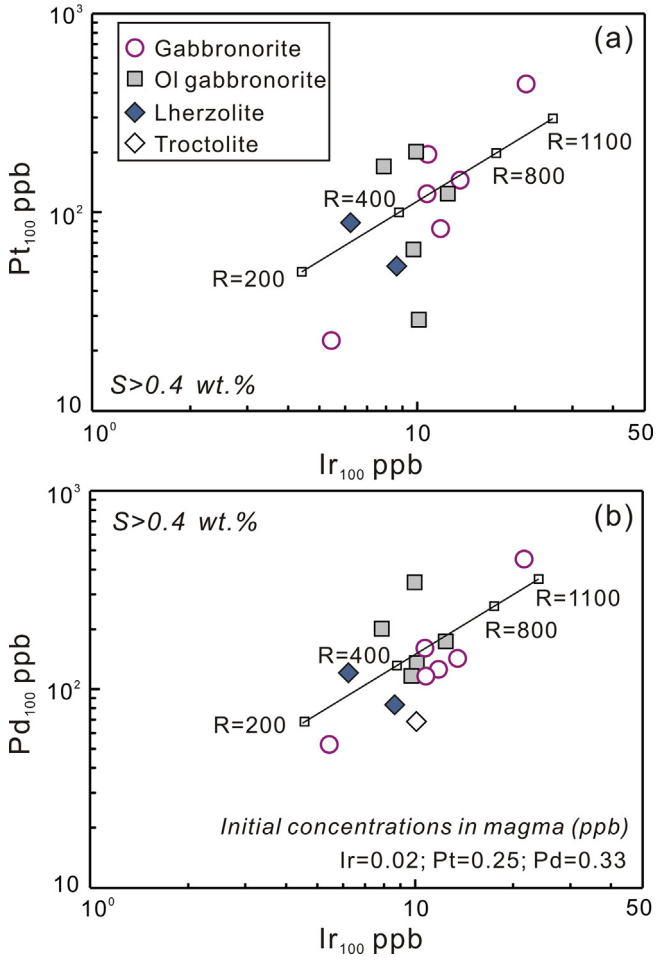

Fig. 13. Plots of Pt versus Ir (a) and Pd versus Ir (b) in recalculated 100% sulfide (i.e., metal tenors) in the Podong magmatic sulfide deposit. R-factors are magma/sulfide mass ratios (Campbell and Naldrett 1979). The details of modeling are given in the text.

liquid, it is difficult to determine the content of Ni in magma. Thus, we have selected Cu for modeling. In the calculation we assumed that the initial content of Cu in the parental magma of the Podong deposit is 100 ppm, which is the upper limit for arc basalts (Lee et al., 2012). This assumption is reasonable, because the mantle source of the Podong magma could have been modified previously by slab-derived fluids or melt. Using an experimental D_{Cu} of 1000 for basaltic system (Ripley et al., 2002; Mungall and Brenan, 2014) and the assumed initial Cu content in magma, we have obtained the minimum R-factor of ~200 for the Podong magmatic sulfide deposit. Based on this value and the recommended D values of 10^5 for PGE (Mungall and Brenan, 2014), the initial concentrations of Ir, Pt and Pd in the Podong magma are estimated to be 0.02 ppb, 0.25 ppb and 0.33 ppb, respectively. These values are about two orders of magnitude lower than those in the PGE-undepleted picritic basalts of the Emeishan flood basalt province (Li et al., 2012, 2016) and the Siberian flood basalt province (Lightfoot and Keays, 2005).

One possible explanation for PGE depletions in magma is previous sulfide segregation at depth (e.g., Barnes and Maier, 1999; Lightfoot and Keays, 2005; Zhang et al., 2011; Gao et al., 2013). Another possibility is sulfide retention in the mantle source due to low degrees of partial melting (Keays, 1995; Lesher and Stone, 1996; Barnes and Maier, 1999; Song et al., 2016). The third possibility is a PGE-depleted mantle source, which was used to explain PGE depletions in the Voisey's Bay magmatic sulfide deposit (Lightfoot et al., 2012). Pt and Pd are incompatible during partial melting in the mantle (Barnes et al.,

1985; Barnes and Maier, 1999). Continuous melting and extraction of a PGE-undepleted mantle would finally produce a refractory mantle source with Pt-Pd depletion (Lorand et al., 2008; Maier et al., 2012). However, available data for mantle samples indicate that the PGE abundances of orogenic peridotites affected by significant extents of melt extraction are generally similar to those of the fertile orogenic peridotites modified by metasomatic refertilization (Barnes et al., 2015; Aulbach et al., 2016).

Previous sulfide segregation will dramatically increase Cu/Pd ratios in the residual magma because the sulfide/silicate melt partition coefficient of Pd (~10^5: Mungall and Brenan, 2014) is much higher than that of Cu (~10^3: Ripley et al., 2002). Cu/Pd ratios for sulfide-bearing samples from the Podong ultramafic bodies range from 48,000 to 5,00,000, significantly higher than the primitive mantle value (Barnes and Maier, 1999), as well as the nearby coeval Poyi deposit that formed from a more primitive magma as indicated by more primitive olivine with Fo contents up to 90 mol% (Xue et al., 2016a). Thus, previous sulfide liquid segregation at depth before the final magma emplacement at Podong is the favored explanation for the low PGE concentrations, but a PGE-depleted mantle source or sulfide retention in the mantle source cannot be completely eliminated.

6.5. Implications for mineral exploration

The results from this study reveal several important signatures which can be key evaluative factors for Ni exploration in the Beishan region. These include: (1) a younger episode of Ni metallogeny in Beishan (~270 Ma) than the adjacent Tianshan to the north (~280 Ma, Fig. 1), (2) widespread sulfide mineralization associated with both primitive and more fractionated mafic-ultramafic intrusions in the Beishan region, (3) possible sulfide saturation and sulfide accumulation at depth, and (4) sulfide transportation during magma ascent. Recognizing the protracted nature of basaltic magmatism and associated Ni metallogeny in a convergent tectonic zone from Beishan to Tianshan is important in regional exploration. The use of age for target selection should be restricted to a small area but not to a large region from Beishan to Tianshan. In the Pobei area, priority should be given to more primitive ultramafic intrusions because these intrusions have better potential of hosting high-Ni tenor sulfide mineralization because their parental magmas were less depleted in Ni as a function of lower degrees of olivine fractional crystallization (Xue et al., 2016a). The implication from the last two observations is that drilling should be focused on potential traps for dense sulfide liquid in the magma pluming system, such as the widen portions or more gently-dipping parts of conduit systems, as exemplified by the Voisey's Bay deposit (Li and Naldrett, 1999).

7. Conclusions

Magmatic zircon crystals from the Podong magmatic sulfide deposit yield a mean U-Pb isotope age of ~270 Ma, identical to the age of the nearby Poyi magmatic sulfide deposit that is associated with more primitive ultramafic rocks. These ages together define a new episode of Ni metallogeny for the Beishan region that is ~10 myr younger than the Tianshan region to the north. Like other Permian mafic-ultramafic intrusions in the Beishan-Tianshan region, the parental magma of the Podong magmatic sulfide deposit was originally derived from a mantle source that was likely modified by previous subduction processes. Fractional crystallization and assimilation of siliceous crustal materials appear to have played a role in triggering sulfide saturation in the Podong magma, although addition of external sulfur cannot be ruled out. The Cu/Pd ratios of the Podong magmatic sulfide deposit are significantly higher than the mantle values, indicating previous sulfide segregation at depth. Like all known Permian magmatic sulfide deposits in the Beishan-Tianshan region, the parental magma of the Podong magmatic sulfide deposit is severely depleted in PGE. The reason for such large-scale PGE depletions remains elusive.

Acknowledgments

This study was financially supported by the China Postdoctoral Science Foundation to Shengchao Xue (2016M600109) and the National Natural Science Foundation of China (Grants 41030424 and 41472075). We thank Heng Wang of the Sixth Geological Team of the Xinjiang Bureau of Geology and Mineral Resources for logistic support of field work, Peng Wang and Jianmin Ding for assistance in sampling, and Xianhua Li, Qiuli Li, Liang Qi, Qian Mao, Yuehong Wang, Dingshuai Xue, and Wenjun Li for guidance in sample analysis. Constructive reviews from two anonymous reviewers and revision guidance from the editors are greatly appreciated.

Appendix A. Supplementary data

Supplementary data associated with this article can be found, in the online version, at https://doi.org/10.1016/j.oregeorev.2018.08.017.

References

Ao, S.J., Xiao, W.J., Han, C.M., Mao, Q.G., Zhang, J.E., 2010. Geochronology and geochemistry of Early Permian mafic-ultramafic complexes in the Beishan area, Xinjiang, NW China: implications for late Paleozoic tectonic evolution of the southern Altaids. Gondwana Res. 18, 466–478.

Aulbach, S., Mungall, J.E., Pearson, D.G., 2016. Distribution and processing of highly siderophile elements in cratonic mantle lithosphere. In: Harvey, J., Day, J.M.D. (Eds.), Highly siderophile and strongly chalcophile elements in high-temperature geochemistry and cosmochemistry. Mineralogical Society of America, Chantilly, Rev. Miner. Geochem., pp. 239–304.

Barnes, S.-J., Naldrett, A.J., Gorton, M.P., 1985. The origin of the fractionation of the platinum group elements in terrestrial magmas. Chem. Geol. 53, 303–332.

Barnes, S.-J., Maier, W., 1999. The fractionation of Ni, Cu and the noble metals in silicate and sulphide liquids. Geol. Assoc. Can. Short Course Notes 13, 69–106.

Barnes, S.-J., Lightfoot, P., 2005. Formation of magmatic nickel-sulfide ore deposits and processes affecting their copper and platinum-group element contents. In: Hedenquist, J.W., Thompson, J.F.H., Goldfarb, R.J., Richards, J.P. (Eds.), Economic geology 100th anniversary volume, pp. 179–213.

Barnes, S.J., Roeder, P.L., 2001. The range of spinel compositions in terrestrial mafic and ultramafic rocks. J. Petrol. 42, 2279–2302.

Barnes, S.J., Godel, B., Gürer, D., Brenan, J.M., Robertson, J., Paterson, D., 2013. Sulfide-olivine Fe-Ni exchange and the origin of anomalously Ni rich magmatic sulfides. Econ. Geol. 108, 1971–1982.

Barnes, S.J., Mungall, J.E., Maier, W.D., 2015. Platinum group elements in mantle melts and mantle samples. Lithos 232, 395–417.

Campbell, I.H., Naldrett, A.J., 1979. The influence of silicate: sulfide ratios on the geochemistry of magmatic sulfides. Econ. Geol. 74, 1503–1506.

Class, C., Le Roex, A.P., 2008. Ce anomalies in Gough Island lavas—trace element characteristics of a recycled sediment component. Earth Planet. Sci. Lett. 265, 475–486.

Gao, J.F., Zhou, M.F., Lightfoot, P.C., Wang, C.Y., Qi, L., Sun, M., 2013. Sulfide saturation and magma emplacement in the formation of the Permian Huangshandong Ni-Cu sulfide deposit, Xinjiang, Northwestern China. Econ. Geol. 108, 1833–1848.

Ghiorso, M.S., Sack, R.O., 1995. Chemical mass transfer in magmatic processes IV. A revised and internally consistent thermodynamic model for the interpolation and extrapolation of liquid-solid equilibria in magmatic systems at elevated temperatures and pressures. Contrib. Mineral. Petrol. 119, 197–212.

Guo, Q., Xiao, W., Windley, B.F., Mao, Q., Han, C., Qu, J., Ao, S., Li, J., Song, D., Yong, Y., 2012. Provenance and tectonic settings of Permian turbidites from the Beishan Mountains, NW China: implications for the Late Paleozoic accretionary tectonics of the southern Altaids. J. Asian Earth Sci. 49, 54–68.

Han, B.F., Ji, J.Q., Song, B., Chen, L.H., Li, Z., 2004. SHRIMP zircon U-Pb ages of Kalatongke No. 1 and Huangshandong Cu-Ni-bearing mafic-ultramafic complexes, North Xinjiang, and geological implications. Chin. Sci. Bull. 49, 2424–2429.

Jahn, B.-M., 2004. The Central Asian Orogenic Belt and growth of the continental crust in the Phanerozoic. Geol. Soc. Lond. Spec. Publ. 226, 73–100.

Jiang, C.Y., Cheng, S.L., Ye, S.F., Xia, M.Z., Jiang, H.B., Dai, Y.C., 2006. Lithogeochemistry and petrogenesis of Zhongposhanbei mafic rock body, at Beishan region. Xinjiang. Acta Petro. Sin. 22, 115–126.

Kamenetsky, V.S., Crawford, A.J., Meffre, S., 2001. Factors controlling chemistry of magmatic spinel: an empirical study of associated olivine, Cr-spinel and melt inclusions from primitive rocks. J. Petrol. 42, 655–671.

Keays, R.R., 1995. The role of komatiitic and picritic magmatism and S-saturation in the formation of the ore deposits. Lithos 34, 1–18.

Lee, C.T.A., Luffi, P., Chin, E.J., Bouchet, R., Dasgupta, R., Morton, D.M., Le Roux, V., Yin, Q.Z., Jin, D., 2012. Copper systematics in arc magmas and implications for crust-mantle differentiation. Science 336, 64–68.

Lesher, C.M., Stone, W.E., 1996. Exploration geochemistry of komatiites. In: Wyman, D.A.

(Ed.), Trace element geochemistry of volcanic rocks: applications for massive sulfide exploration. Geolog. Assoc. Can. Short Course Notes, pp. 153–204.
Li, C., Naldrett, A.J., 1999. The geology and petrology of the Voisey's Bay intrusion: reaction of olivine with trapped sulfide and silicate liquids. Lithos 47, 1–31.
Li, C., Ripley, E.M., 2010. The relative effects of composition and temperature on olivine-liquid Ni partitioning: statistical deconvolution and implications for petrologic modeling. Chem. Geol. 275, 99–104.
Li, C., Ripley, E.M., 2011. The giant Jinchuan Ni-Cu-(PGE) deposit: tectonic setting, magma evolution, ore genesis and exploration implications. Rev. Econ. Geol. 17, 163–180.
Li, C., Barnes, S.J., Makovicky, E., Rose-Hansen, J., Makovicky, M., 1996. Partitioning of nickel, copper, iridium, rhenium, platinum, and palladium between monosulfide solid solution and sulfide liquid: effects of composition and temperature. Geochim. Cosmochim. Acta 60, 1231–1238.
Li, C., Naldrett, A.J., Ripley, E.M., 2007. Controls on the Fo and Ni contents of olivine in sulfide-bearing mafic/ultramafic intrusions: principles, modeling and examples from Voisey's Bay. Earth Sci. Front. 14, 177–185.
Li, C., Tao, Y., Qi, L., Ripley, E.M., 2012. Controls on PGE fractionation in the Emeishan picrites and basalts: constraints from integrated lithophile-siderophile elements and Sr-Nd isotopes. Geochim. Cosmochim. Acta 90, 12–32.
Li, C., Ripley, E.M., Thakurta, J., Stifter, E.C., Qi, L., 2013. Variations of olivine Fo-Ni contents and highly chalcophile element abundances in arc ultramafic cumulates, southern Alaska. Chem. Geol. 351, 15–28.
Li, C., Zhang, Z.W., Li, W.Y., Wang, Y.L., Sun, T., Ripley, E.M., 2015. Geochronology, petrology and Hf-S isotope geochemistry of the newly-discovered Xiarihamu magmatic Ni-Cu sulfide deposit in the Qinghai-Tibet plateau, western China. Lithos 216, 224–240.
Li, C., Ripley, E.M., Tao, Y., Hu, R., 2016. The significance of PGE variations with Sr-Nd isotopes and lithophile elements in the Emeishan flood basalt province from SW China to northern Vietnam. Lithos 248–251, 1–11.
Li, X.H., Liu, Y., Li, Q.L., Guo, C.H., Chamberlain, K.R., 2009. Precise determination of Phanerozoic zircon Pb/Pb age by multi-collector SIMS without external standardization. Geochem. Geophys. Geosys. 10, 1–21.
Li, X.H., Li, W.X., Li, Q.L., Wang, X.C., Liu, Y., Yang, Y.H., 2010. Petrogenesis and tectonic significance of the 850 Ma Gangbian alkaline complex in South China: evidence from in situ zircon U-Pb dating, Hf-O isotopes and whole-rock geochemistry. Lithos 114, 1–15.
Lightfoot, P.C., Keays, R.R., 2005. Siderophile and chalcophile metal variations in flood basalts from the Siberian trap, Noril'sk region: implications for the origin of the Ni-Cu-PGE sulfide ores. Econ. Geol. 100, 439–462.
Lightfoot, P.C., Keays, R.R., Evans-Lamswood, D.S., Wheeler, R., 2012. S saturation history of Nain Plutonic Suite mafic intrusions: origin of the Voisey's Bay Ni-Cu-Co sulfide deposit, Labrador, Canada. Miner. Deposita 47, 23–50.
Liu, Y.S., Zong, K.Q., Kelemen, P.B., Gao, S., 2008. Geochemistry and magmatic history of eclogites and ultramafic rocks from the Chinese continental scientific drill hole: subduction and ultrahigh-pressure metamorphism of lower crustal cumulates. Chem. Geol. 247, 133–153.
Lorand, J.P., Luguet, A., Alard, O., Bezos, A., Meisel, T., 2008. Abundance and distribution of platinum-group elements in orogenic lherzolites; a case study in a Fontete Rouge lherzolite (French Pyrénées). Chem. Geol. 248, 174–194.
Ludwig, K.R., 2012. User's Manual for Isoplot 3.75: a geochronological toolkit for Microsoft Excel. Berkeley Geochronology Centre Spec. Pub. No. 5, 75.
Ma, J., Lü, X., Liu, Y., Cao, X., Liu, Y., Ruan, B., Adam, M.M.A., 2016. The impact of early sulfur saturation and calc-crustal contamination on ore-forming process in the Posan mafic-ultramafic complex: derived from the shallow depleted mantle, Beishan region, NW China. J. Asian Earth Sci. 118, 81–94.
Maier, W.D., Peltonen, P., McDonald, I., Barnes, S.J., Barnes, S.-J., Hatton, C., Viljoen, F., 2012. The concentration of platinum-group elements and gold in southern African and Karelian kimberlite-hosted mantle xenoliths: implications for the noble metal content of the Earth's mantle. Chem. Geol. 302–303, 119–135.
Mao, Y.J., Qin, K.Z., Li, C., Xue, S.C., Ripley, E.M., 2014. Petrogenesis and ore genesis of the Permian Huangshanxi sulfide ore-bearing mafic-ultramafic intrusion in the Central Asian orogenic belt, western China. Lithos 200, 111–125.
Mao, Y.J., Qin, K.Z., Li, C., Tang, D.M., 2015. A modified genetic model for the Huangshandong magmatic sulfide deposit in the Central Asian Orogenic Belt, Xinjiang, western China. Miner. Deposita 50, 65–82.
Mao, Y.J., Qin, K.Z., Tang, D.M., Feng, H.Y., Xue, S.C., 2016. Crustal contamination and sulfide immiscibility history of the Permian Huangshannan magmatic Ni-Cu sulfide deposit, East Tianshan, NW China. J. Asian Earth Sci. 129, 22–37.
Matzen, A.K., Baker, M.B., Beckett, J.R., Stolper, E.M., 2011. Fe-Mg partitioning between olivine and high-magnesian melts and the nature of Hawaiian parental liquids. J. Petrol. 52, 1243–1263.
Mungall, J.E., Brenan, J.M., 2014. Partitioning of platinum-group elements and Au between sulfide liquid and basalt and the origins of mantle-crust fractionation of the chalcophile elements. Geochim. Cosmochim. Acta 125, 265–289.
Naldrett, A.J., 2011. Fundamentals of magmatic sulfide deposits. Rev. Econ. Geol. 17, 1–50.
Nielsen, R.L., Beard, J.S., 2000. Magnetite-melt HFSE partitioning. Chem. Geol. 164, 21–34.
Palme, H., O'Neill, H.S.C., 2014. Cosmochemical estimates of mantle composition. In: In: Holland, H.D., Turekian, K.K. (Eds.), Treatise on Geochemistry Vol. 3. Elsevier, pp. 1–38.
Prichard, H.M., Knight, R.D., Fisher, P.C., McDonald, I., Zhou, M.-F., Wang, C.Y., 2013. Distribution of platinum-group elements in magmatic and altered ores in the Jinchuan intrusion, China: an example of selenium remobilization by post magmatic fluids. Miner. Deposita 48, 767–786.
Qi, L., Zhou, M.-F., Wang, C.Y., Sun, M., 2007. Evaluation of a technique for determining Re and PGEs in geological samples by ICP-MS coupled with amodified Carius tube digestion. Geochem. J. 41, 407–414.
Qi, L., Gao, J.F., Huang, X.W., Hu, J., Zhou, M.F., Zhong, H., 2011. An improved digestion technique for determination of platinum group elements in geological samples. J. Ana. Atom. Spectrom. 26, 1900–1904.
Qin, K.Z., Su, B.X., Sakyi, P.A., Tang, D.M., Li, X.H., Sun, H., Xiao, Q.H., Liu, P.P., 2011. SIMS zircon U-Pb geochronology and Sr-Nd isotopes of Ni-Cu-bearing mafic-ultramafic intrusions in eastern Tianshan and Beishan in correlation with flood basalts in Tarim Basin (NW China): constraints on a ca. 280 Ma mantle plume. Am. J. Sci. 311, 237–260.
Ripley, E.M., Brophy, J.G., Li, C., 2002. Copper solubility in a basaltic melt and sulfide liquid/silicate melt partition coefficients of Cu and Fe. Geochim. Cosmochim. Acta 66, 2791–2800.
Ripley, E.M., Li, C., 2013. Sulfide saturation in mafic magmas: is external sulfur required for magmatic Ni-Cu-(PGE) ore genesis? Econ. Geol. 108, 45–58.
Rudnick, R.L., Gao, S., Ling, W.L., Liu, Y.S., Mcdonough, W.F., 2004. Petrology and geochemistry of spinel peridotite xenoliths from Hannuoba and Qixia, North China craton. Lithos 77, 609–637.
Song, D.F., Xiao, W.J., Han, C.M., Tian, Z.H., Wang, Z.M., 2013. Provenance of metasedimentary rocks from the Beishan orogenic collage, southern Altaids: constraints from detrital zircon U-Pb and Hf isotopic data. Gondwana Res. 24, 1127–1151.
Song, X.Y., Xie, W., Deng, Y.F., Crawford, A.J., Zheng, W.Q., Zhou, G.F., Deng, G., Chen, S.L., Li, J., 2011. Slab break-off and the formation of Permian mafic-ultramafic intrusions in southern margin of Central Asian Orogenic Belt, Xinjiang, NW China. Lithos 127, 128–143.
Song, X.Y., Yi, J.N., Chen, L.M., She, Y.W., Liu, C.Z., Dang, X.Y., Yang, Q.A., Wu, S.K., 2016. The Giant Xiarihamu Ni-Co Sulfide Deposit in the East Kunlun Orogenic Belt, Northern Tibet Plateau. China. Econ. Geol. 111, 29–55.
Studley, S.A., Ripley, E.M., Elswick, E.R., Dorais, M.J., Fong, J., Finkelstein, D., Pratt, L.M., 2002. Analysis of sulfides in whole rock matrices by elemental analyzer-continuous flow isotope ratio mass spectrometry. Chem. Geol. 192, 141–148.
Su, B.X., Qin, K.Z., Tang, D.M., Sakyi, P.A., Liu, P.P., Sun, H., Xiao, Q.H., 2013. Late Paleozoic mafic-ultramafic intrusions in southern Central Asian Orogenic Belt (NW China): insight into magmatic Ni-Cu sulfide mineralization in orogenic setting. Ore Geol. Rev. 51, 57–73.
Tang, D.M., Qin, K.Z., Li, C., Qi, L., Su, B.X., Qu, W.J., 2011. Zircon dating, Hf-Sr-Nd-Os isotopes and PGE geochemistry of the Tianyu sulfide-bearing mafic-ultramafic intrusion in the Central Asian Orogenic Belt, NW China. Lithos 126, 84–98.
Thakurta, J., Ripley, E.M., Li, C., 2008. Geochemical constraints on the origin of sulfide mineralization in the Duke Island Complex, southeastern Alaska. Geochem. Geophys. Geosys. 9, 3562–3585.
Wang, G.Q., 2015. The research of the Paleozoic ophiolites and volcanic rocks and the tectonic evolution in the Beishan area (northwest China). Dissertation, Chang'an University.
Xia, M.Z., Jiang, C.Y., Li, C., Xia, Z.D., 2013. Characteristics of a newly discovered Ni-Cu sulfide deposit hosted in the Poyi ultramafic intrusion, Tarim craton, NW China. Econ. Geol. 108, 1865–1878.
Xiao, W.J., Windley, B.F., Badarch, G., Sun, S., Li, J.L., Qin, K.Z., Wang, Z., 2004. Palaeozoic accretionary and convergent tectonics of the southern Altaids: implications for the growth of central Asia. J. Geol. Soc. Lond. 161, 339–342.
Xiao, W.J., Mao, Q.G., Windley, B.F., Han, C.M., Qu, J.F., Zhang, J.E., Ao, S.J., Guo, Q.Q., Cleven, N.R., Lin, S.F., Shan, Y.H., Li, J.L., 2010. Paleozoic multiple accretionary and collisional processes of the Beishan orogenic collage. Am. J. Sci. 310, 1553–1594.
Xue, S.C., Qin, K.Z., Li, C., Tang, D.M., Mao, Y.J., Qi, L., Ripley, E.M., 2016a. Geochronological, petrological, and geochemical constraints on Ni-Cu sulfide mineralization in the Poyi ultramafic-troctolitic intrusion in the northeast rim of the Tarim craton, western China. Econ. Geol. 111, 1465–1484.
Xue, S.C., Li, C., Qin, K.Z., Tang, D.M., 2016b. A non-plume model for the Permian protracted (266–286Ma) basaltic magmatism in the Beishan-Tianshan region, Xinjiang, Western China. Lithos 256, 243–249.
Yang, S.H., Zhou, M.F., Lightfoot, P., Xu, J.F., Wang, C., Jiang, C.Y., Qu, W.J., 2014. Re-Os isotope and platinum-group element geochemistry of the Pobei Ni-Cu sulfide-bearing mafic-ultramafic complex in the northeastern part of the Tarim craton. Miner. Deposita 49, 381–397.
Yue, Y., Liou, J.G., Graham, S.A., 2001. Tectonic correlation of Beishan and Inner Mongolia orogens and its implications for the palinspastic reconstruction of north China. Geol. Soc. Am. Mem. 194, 101–116.
Zhang, M.J., Li, C., Fu, P., Hu, P.Q., Ripley, E.M., 2011. The Permian Huangshanxi Cu-Ni deposit in western China: intrusive-extrusive association, ore genesis, and exploration implications. Miner. Deposita 46, 153–170.
Zhang, Y.Y., Guo, Z.J., 2008. Accurate constraint on formation and emplacement age of Hongltuhe ophiolite, boundary region between Xinjiang and Gansu Provinces and its tectonic implications. Acta Petrol. Sin. 24, 803–809.
Zhao, Y., Xue, C.J., Zhao, X.B., Yang, Y.Q., Ke, J.J., 2015. Magmatic Cu-Ni sulfide mineralization of the Huangshannan mafic-ultramafic intrusion, Eastern Tianshan. China. J. Asian Earth Sci. 105, 155–172.
Zindler, A., Hart, S.R., 1986. Chemical geodynamics. Annu. Rev. Earth Planet. Sci. 14, 493–571.
Zuo, G., Li, M., 1996. Formation and evolution of the Early Paleozoic lithosphere in the Beishan area. Gansu Science and Technology Press, Gansu-Inner Mongolia, China, pp. 120.
Zuo, G., Zhang, S., He, G., Zhang, Y., 1990. Early Paleozoic plate tectonics in Beishan area. Chin. J. Geol. 4, 305–315.